Chapter 11

Planar Antennas for Reliable Multiband RF Communications

Mohammad Alibakhshikenari,
Mohammad Naser-Moghadasi,
Ramazan Ali Sadeghzadeh, Bal Singh Virdee and
Ernesto Limiti

Additional information is available at the end of the chapter

http://dx.doi.org/10.5772/66675

Abstract

Multiband functionality in antennas has become a fundamental requirement to equip wireless devices with multiple communication standards so that they can utilize the electromagnetic spectrum more efficiently and effectively. This is necessary to ensure global portability and enhance system capacity. To meet these requirements, microstrip technology is increasingly being used in communication systems because it offers considerable size reduction, cost-effectiveness as they can be easily manufactured in mass production, are durable and can conform to planar or cylindrical surfaces. Unfortunately, such antennas suffer from intrinsically narrow bandwidth. To overcome this deficiency, various techniques have been investigated in the past. In this chapter, a novel approach is presented to design antennas for applications that cover radio frequency identification (RFID) and WiMAX systems.

Keywords: planar antenna, meandered strip-line feed, wideband antenna, multiband antenna

1. Introduction

Innovative design concepts that have been facilitated by cutting-edge technology are contributing toward boosting wireless communications. Antennas are an essential component in such systems; however the large dimensions and narrow operating range of conventional antennas preclude them from application in the next generation of wireless communications systems. This is because future wireless systems impose strict requirements from antennas, such as

large impedance bandwidth to support multiple systems, small physical size, low cost designs, high efficiency and reliability.

To utilize the electromagnetic spectrum more efficiently and effectively it has become necessary to equip portable wireless devices with multiple communication standards. This necessitates antennas to operate over a wideband [1, 2]. Nowadays microstrip integrated technology (MIT) is being increasingly used in the design of antennas for application in wireless communication systems because it offers considerable size reduction, cost effectiveness as it allows easy manufacture in mass production, durability and enables antennas to be configured for mounting on various irregular surfaces [3, 4]. Unfortunately, such antennas have intrinsically narrow bandwidth. To circumvent this deficiency, numerous techniques have been investigated recently, which include embedding slit-lines in the patch antenna [5–9]; employing unconventional feeding structures [10, 11]; insertion of parasitic elements in the vicinity of the patch antenna [12]; employing thick substrates and/or higher dielectric constant substrates [13, 14]; loading the antenna with an arrangement of electromagnetic band-gap (EBG) structures [15]; using meta-surfaces [16] and employing metamaterial (MTM) unit cells [17–19]. These techniques certainly improve the impedance bandwidth of antennas; however, it is not sufficient to support multiple wireless communications systems. Another interesting technique to enhance the bandwidth of patch antennas uses meandered strip-line feed which has the advantage of being less complex to implement in practice [20].

In this chapter, a planar microstrip antenna is proposed for multiband wireless communications systems. Embedded in the antenna's radiation patch are an H-shaped slit and two inverted U-shaped capacitive slits. The antenna is fed through a meandered strip-line. The antennas described in this chapter are fabricated on RT/duroid® RO4003 substrate with permittivity of 3.38, thickness of 1.6 mm and $\tan\delta = 0.0022$. The final second antenna occupies an area of 13.5 mm × 12.7 mm or $0.036\lambda_0 \times 0.033\lambda_0$, where the free space wavelength (λ_0) is 0.8 GHz. Numerical parametric analyses was used to (1) determine the location of the slits in the rectangular patch and (2) the optimum meandered-line feed structure. Verification of the antenna performance was done through measurement. It will be shown later the proposed antenna exhibits properties of low radiation loss, low cross-polarization, ease of manufacture and integration in RF transceivers, and no use via holes. These characteristics make it suitable for multiband applications, such as Ultra High Frequency (UHF) Radio Frequency Identification (RFID), Global Positioning System (GPS), Personal Communication Systems (PCS), Digital Communication Systems (DCS), Worldwide Interoperability for Microwave Access (WiMAX), Wireless Local Area Network (WLAN), WiFi, Bluetooth and other applications in the UHF, L, S, major part of C-bands.

2. MTM antenna design

The design technique described in this chapter offers expansion of the impedance bandwidth of the antenna without compromising its size and salient characteristics. This is achieved by inserting dielectric slits in the antenna patch and exciting it through a meandered strip-line. The antenna design employs an H-shape and inverted U-shape slit.

To minimize design complexity and reduce manufacturing cost the proposed antenna structure avoids the use of via-holes.

http://dx.doi.org/10.5772/66675

2.1. H-shaped slit patch antenna

The generic patch antenna configuration and its equivalent circuit model are shown in **Figure 1**. The slit essentially behave as series capacitor (C_L) and the meandered microstrip feed-line behaves as a shunt inductor (L_L). Other losses introduced by the antenna structure are represented by series right-handed resistance (R_R), shunt left-handed resistance (R_L), series conductance (G_L) and shunt conductance (G_R). Location and dimensions of the slit was optimized using 3D electromagnetic high frequency structural simulator (HFSS™) by ANSYS [21]. The electromagnetic fields and currents are concentrated in the vicinity of the patch by placing the slit at the center of patch. This prevents the fields from spreading on the ground plane of the antenna and thereby minimizes unwanted coupling. This technique contributes in the realization of a smaller patch antenna. The use of this antenna structure in an array would incur minimal mutual coupling which is important to de-correlate multipath channels in, for example, small cellular systems. The meandered microstrip feed-line ensures low radiation loss and low cross-polarization. It also helps to eliminate unwanted notch bands in the antenna's response due to impedance mismatch, thus providing bandwidth extension.

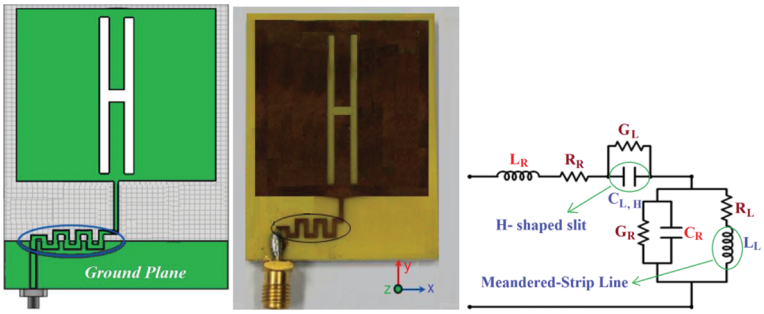

Figure 1. Configuration of the antenna constructed using an H-shaped slit and meandered microstrip feed-line, (a) simulation model, (b) fabricated prototype and (c) equivalent circuit model.

Length (L), width (W) and height (h) of the proposed antenna are 21.2 mm, 15 mm and 1.6 mm, respectively. The length (L_p) and width (W_p) of radiation patch are 13.5 mm and 12.7 mm, respectively. The corresponding electrical size of the antenna and radiation patch is $0.155\lambda_o \times 0.110\lambda_o \times 0.011\lambda_o$ and $0.099\lambda_o \times 0.093\lambda_o$, respectively, where λ_o is free space wavelength at 2.2 GHz. The antenna's simulated and measured reflection-coefficient (S_{11}) response is shown in **Figure 2**. The simulated impedance bandwidth of the antenna for $S_{11} < -10$ dB is 2.58 GHz (2.05–4.63 GHz), and a fractional bandwidth of 77.2%. The antenna has a measured bandwidth of 2.3 GHz (2.2–4.5 GHz), and a fractional bandwidth of 68.7%. The simulated result shows the antenna to resonate at $f_{r,sim}$ = 3.6 GHz3.6 GHz, which is very close to the measured result at $f_{r,measured}$ = 3.5 GHz3.5 GHz. The discrepancy between the simulated and measured bandwidth is attributed to manufacturing tolerance and imperfect soldering of the SMA connector.

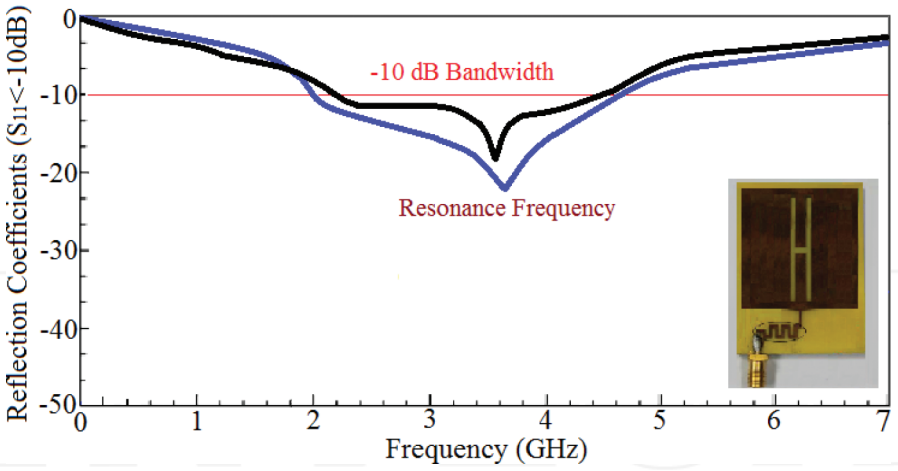

Figure 2. Simulated (blue line) and measured (black line) reflection-coefficient response of the antenna.

The measured gain and radiation efficiency of the antenna at spot frequencies of 2.2, 3.55 and 4.5 GHz are 0.65 dBi and 18.34%, 2.75 dBi and 47.15% and 1.90 dBi and 36.12%, respectively. The optimum measured gain and radiation efficiency of the antenna are 2.75 dBi and 45.15%, respectively, as shown in **Figure 3**, at f_r = 3.55 GHz3.55 GHz.

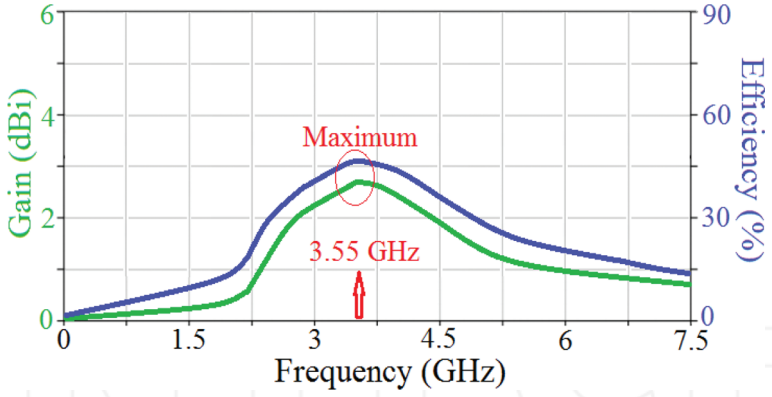

Figure 3. Measured gain and radiation efficiency response of the antenna.

Figure 4 shows the measured co-polarization and cross-polarization radiation patterns in the E(yz) and H(xz) planes at its resonance frequency of f_r = 3.55 GHz3.55 GHz. The measured radiation pattern shows the antenna radiates omni-directionally in the E-plane and bi-directionally in the H-plane. The copolarization and cross-polarization patterns are similar to a typical monopole antenna.

http://dx.doi.org/10.5772/66675

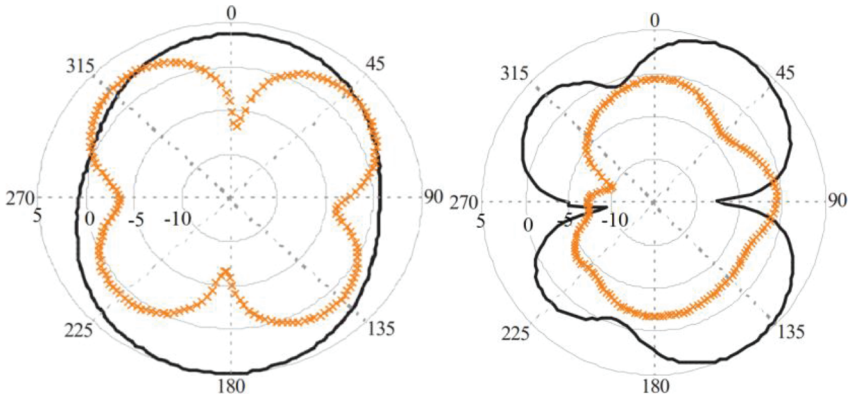

Figure 4. Measured radiation patterns of the antenna at the resonance frequency of 3.55 GHz [Solid line: co-polarization, and crossed line: cross-polarization].

2.2. Patch antenna with inverted U-shape slits located on either of the H-shape slit

The above antenna was modified to improve its performance by inserting two inverted U-shaped slits on either side of the H-shape slit, as shown in **Figures 5** and **6**. The dimensions of the antenna structure are given in **Table 1**. The equivalent circuit model of the proposed symmetrical antenna structure inset in **Figure 7** consists of the composite right/left-handed transmission-line (CRLH-TL), where parasitic series reactance is represented by inductor L_R and shunt capacitor C_R. Series resonance is due to L_R and C_L, and shunt resonance due to C_R and L_L. At low frequency, C_L and L_L dominate and the transmission-line circuit exhibits left-handed characteristics; at high frequency, L_R and C_R dominate and the transmission-line circuit exhibits right-handed characteristics. The propagation constant of the resulting structure is given by Refs. [22–30]:

$$\gamma = \alpha + j\beta = \sqrt{ZY} \tag{1}$$

With

$$\beta(\omega) = s(\omega)\sqrt{\omega^2 L_R C_R + \frac{1}{\omega^2 L_L C_L} - \left(\frac{L_R}{L_L} + \frac{C_R}{C_L}\right)} \tag{2}$$

Where

$$s(\omega) = \begin{cases} -1 \text{ if} \omega < \omega_{se} = \min\left(\frac{1}{\sqrt{L_R C_L}}, \frac{1}{\sqrt{L_L C_R}}\right) \\ 0 \text{ if} \omega_{se} < \omega < \omega_{sh} \\ +1 \text{ if} \omega > \omega_{sh} = \max\left(\frac{1}{\sqrt{L_R C_L}}, \frac{1}{\sqrt{L_L C_R}}\right) \end{cases} \quad (3)$$

and

$$Z(\omega) = j(\omega L_R - 1/\omega C_L) \quad (4)$$

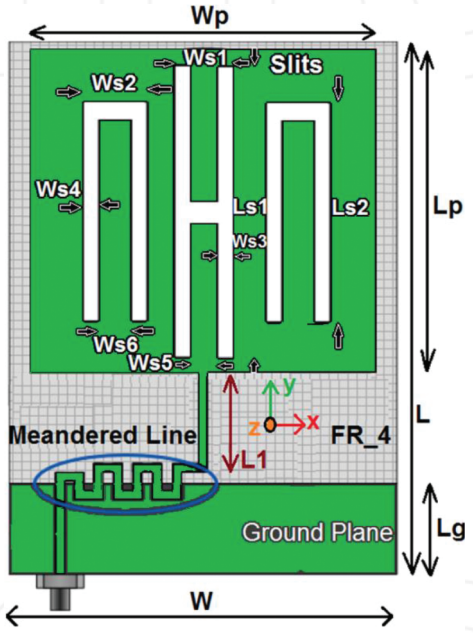

(a)

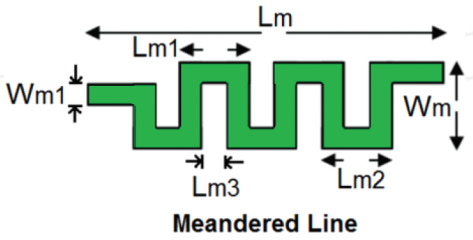

(b)

Figure 5. (a) Geometry of the MTM antenna and (b) meandered strip-line feed.

http://dx.doi.org/10.5772/66675

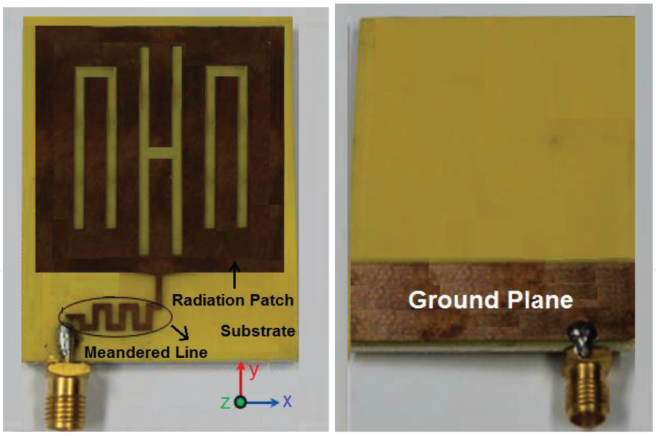

Figure 6. Fabricated prototype MTM antenna.

Dimensions (millimeters)									
L	W	W_p	L_p	L_g	L_{s1}	L_{s2}	W_{s1}	W_{s2}	W_{s3}
21.2	15	12.7	13.5	3.6	12	8.5	2.4	2.4	0.6
W_{s4}	W_{s5}	W_{s6}	L_1	L_m	L_{m1}	L_{m2}	L_{m3}	W_{m1}	W_m
0.6	1.2	1.2	3.5	4.5	0.9	0.9	0.3	0.3	1.2
Equivalent circuit Components (pF, nH, Ω, S)									
$C_{L,H}$	$C_{L,\pi Left}$	$C_{L,\pi Right}$	C_R	L_L	L_R	R_L	R_R	G_L	G_R
4.5	3.1	3.1	2	5.1	2.3	1.6	0.8	1.3	0.5

Table 1. Structural parameters of the proposed antenna and meandered strip-line feed.

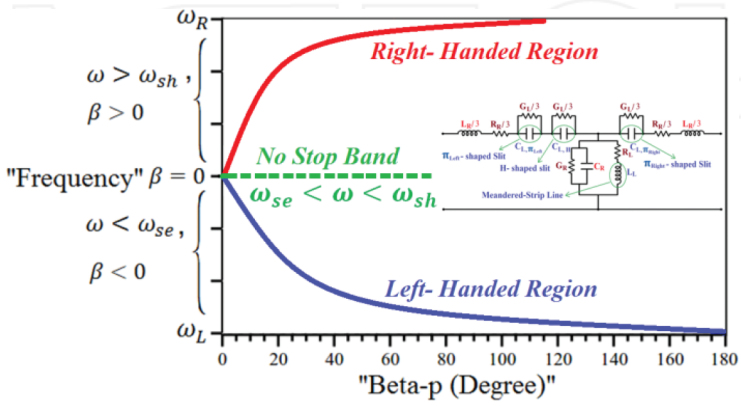

Figure 7. Dispersion diagram.

$$Y(\omega) = j(\omega C_R - 1/\omega L_L) \tag{5}$$

Parameters $\beta(\omega)$, $s(\omega)$, $Z(\omega)$ and $Y(\omega)$ are a function of frequency and represent dispersion, sign function, impedance and admittance of the antenna structure, respectively. The series and shunt resonance frequencies are given by:

$$\omega_{se} = \frac{1}{\sqrt{L_R C_L}} \tag{6}$$

$$\omega_{sh} = \frac{1}{\sqrt{L_L C_R}} \tag{7}$$

The phase and group velocities are given by:

$$v_p = \frac{\omega}{\beta} = \omega^2 \sqrt{L_L C_L} \tag{8}$$

$$v_g = \left(\frac{\partial \beta}{\partial \omega}\right)^{-1} = \omega^2 \sqrt{L_L C_L} \tag{9}$$

The antenna's dispersion diagram in **Figure 7** shows the bandwidth of structure changes from high-pass left-handed response with cut-off frequency ω_L to low-pass right-handed response with cut-off frequency ω_R with no obvious stop-band. The cut-off frequencies ω_L and ω_R are given by:

$$\omega_L = \frac{1}{\sqrt{L_L C_L}} \tag{10}$$

$$\omega_R = \frac{1}{\sqrt{L_R C_R}} \tag{11}$$

Individual slits embedded in the antenna resonate at specific frequencies, as shown in **Figure 8**. The resonance at 2.05 GHz is generated by the inverted U-slit on the left-hand side of the H-slit; the resonance at 3.7 GHz is generated by the H-slit and the resonance at 4.45 GHz results from the inverted U-slit on the right-hand side of the H-slit. Simulated and measured impedance bandwidth of the proposed antenna are 5.55 GHz (0.65–6.2 GHz) and 5.25 GHz (0.8–6.05 GHz), respectively; and the corresponding fractional bandwidths are 162.04 and 153.28%, respectively. These results confirm the antenna can operate over multiple wireless communications standards, in particular, UHF RFID, WLAN, WiMAX, WiFi, Bluetooth, GPS, PCS, and

http://dx.doi.org/10.5772/66675

DCS [31, 32]. Electrical size of the antenna at 800 MHz is $0.056\lambda_o \times 0.040\lambda_o \times 0.004\lambda_o$, which makes it eligible for application in various wireless systems.

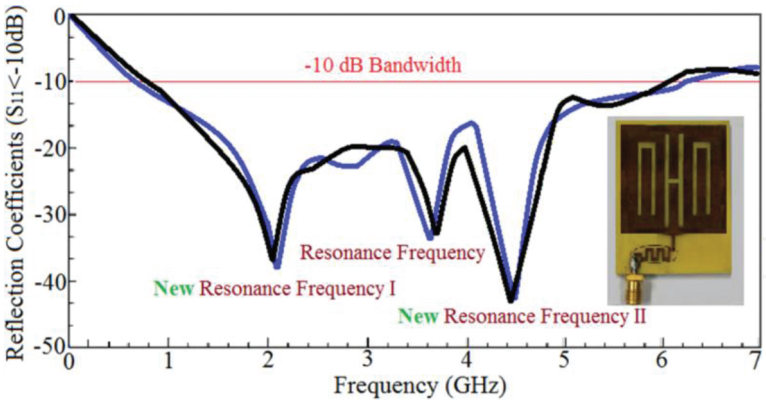

Figure 8. Simulated (blue line) and measured (black line) reflection-coefficient response of the MTM antenna.

The measured gain and radiation efficiency of the antenna in **Figure 9** at 0.8, 2.05, 3.7, 4.45 and 6.05 GHz are 0.95 dBi and 25.8%, 3.85 dBi and 63.1%, 4.73 dBi and 75.9%, 5.35 dBi and 84.1% and 3.05 dBi and 50.2%, respectively. The optimum gain and radiation efficiency of the antenna are 5.35 dBi and 84.1% at 4.45 GHz. **Figure 10** shows the antenna's measured radiation pattern at spot frequencies.

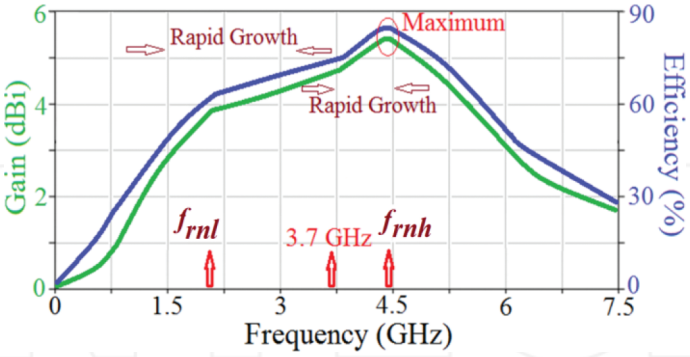

Figure 9. Measured gain and radiation efficiency of the MTM antenna.

The radiation field in the E-plane is omni-directional however this deteriorates at the first resonance frequency of 2.05 GHz. In the H-plane the antenna radiates bi-directionally across its operational bandwidth. This antenna provides the best cross-polarization compared to the above antennas. The current distribution over the antenna at its three resonance frequencies is shown in **Figure 11**.

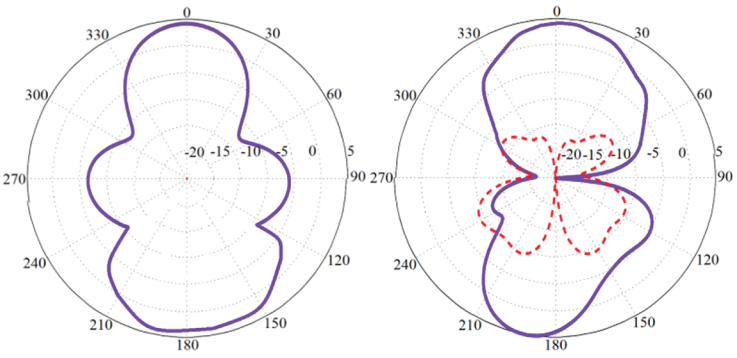

E(yz)-plane H(xz)-plane

At f_{r1} =2.05 GHz, due the left-hand side inverted U-slit

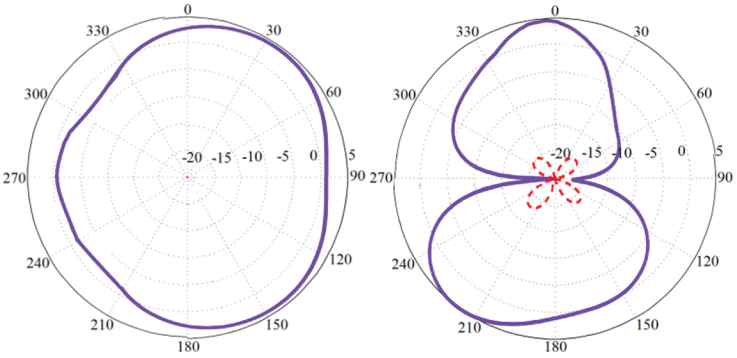

E(yz)-plane H(xz)-plane

At f_{r2} =3.7 GHz, due the middle H-slit

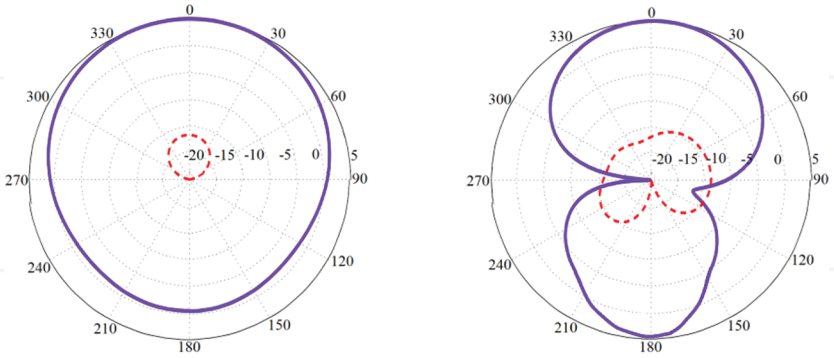

E(yz)-plane H(xz)-plane

At f_{r3} = 4.45 GHz, due the right-hand side inverted U-slit

Figure 10. Measured radiation patterns of the MTM antenna at 2.05, 3.7 and 4.45 GHz [Solid line: copolarizations, and dashed line: cross-polarizations]. Note: in some E-plane patterns the cross-polarization is not visible it is well below −30 dB.

http://dx.doi.org/10.5772/66675

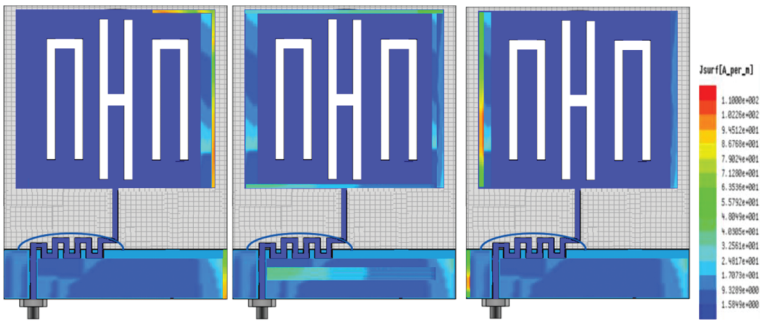

Figure 11. Current density distribution over the MTM antenna at various spot frequencies. (a) f_{r1} = 2.05 GHz; (b) f_{r2} = 3.5 GHz; (c) f_{r3} = 4.45 GHz.

3. Parametric study

A parametric study is necessary to understand the effect of the slits and the meandered stripline feed on the characteristics of the second antenna. The results in **Figure 12** shows that the length (L_{S1}) and width (W_{S3}) of H-shaped slit can substantially improve the impedance bandwidth of the antenna. Salient results are given in **Table 2** where all other structural parameters were kept fixed.

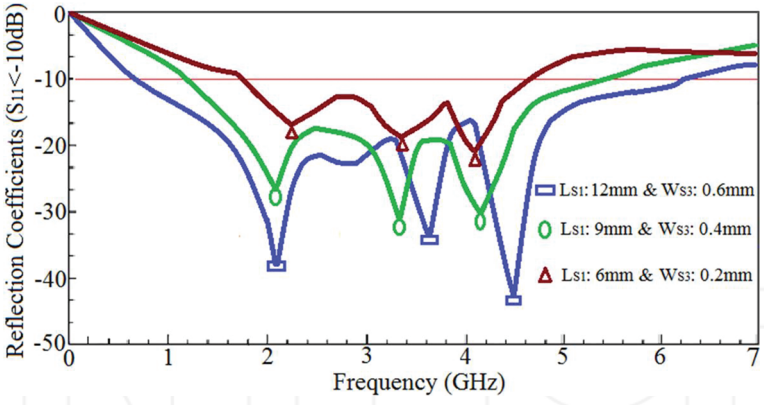

Figure 12. Effect on the antenna impedance bandwidth as a function of H-slit length (L_{S1}) and width (W_{S3}). All other structural parameters given in **Table 1** remain fixed.

The effect of inverted U-shaped slit's length (L_{S2}) and width (W_{S4}) on the antenna is shown in **Figure 13**. **Figure 13** shows that by increasing L_{S2} and W_{S4} of the two inverted U-shaped slits the impedance bandwidth and impedance match of the antenna are improved significantly. The results of this analysis are given in **Table 3**.

Length and width	Frequency bandwidth
L_{S1} = 6 mm & W_{S3} = 0.2 mm	1.75–4.63 GHz ≈90.28%, S_{11} better than −20 dB
	f_{r1} = 2.25, f_{r2} = 3.38 and f_{r3} = 4.1 GHz
L_{S1} = 9 mm & W_{S3} = 0.4 mm	1.2–5.47 GHz ≈128.03%, S_{11} better than −30 dB
	f_{r1} = 2.1, f_{r2} = 3.35 and f_{r3} = 4.15 GHz
L_{S1} = 12 mm & W_{S3} = 0.6 mm	0.65–6.2 GHz ≈162.04%, S_{11} better than −40 dB
	f_{r1} = 2.1, f_{r2} = 3.65 and f_{r3} = 4.5 GHz

Table 2. Effect of length and width of H-shaped slit on the antenna bandwidth.

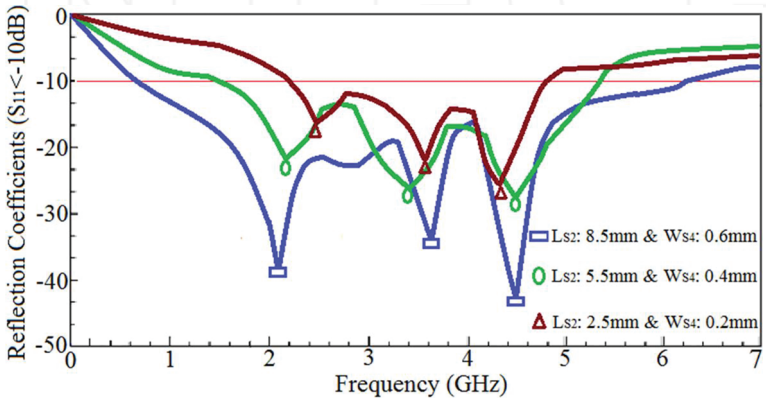

Figure 13. Parametric study on the antenna as a function of length (L_{S2}) and width (W_{S4}) of the inverted U-shaped slits. All other structural parameters in **Table 1** remain fixed.

Length and width	Frequency bandwidth
L_{S2} = 2.5 mm & W_{S4} = 0.2 mm	2.2–4.8 GHz ≈74.28%, S_{11} better than −20 dB
	f_{r1} = 2.48, f_{r2} = 3.58 and f_{r3} = 4.34 GHz
L_{S2} = 5.5 mm & W_{S4} = 0.4 mm	1.46–5.37 GHz ≈114.49%, S_{11}better than −30 dB
	f_{r1} = 2.2, f_{r2} = 3.2 and f_{r3} = 4.48 GHz
L_{S2} = 8.5 mm & W_{S4} = 0.6 mm	0.65–6.2 GHz ≈162.04%, S_{11} better than −40 dB
	f_{r1} = 2.1, f_{r2} = 3.65 and f_{r3} = 4.5 GHz

Table 3. Effect of length and width of the inverted U-shaped slits on the antenna bandwidth.

The effect on the antenna's performance by the meandered microstrip feed-line in **Figure 14** shows that it greatly contributes toward improving its impedance match. In fact by increasing the length of L_m, L_{m1} and L_{m2}, the width of W_m has virtually no effect on the impedance

http://dx.doi.org/10.5772/66675

bandwidth of the antenna, however it significantly improves the antenna's impedance match. Details of these results are provided in **Table 4**.

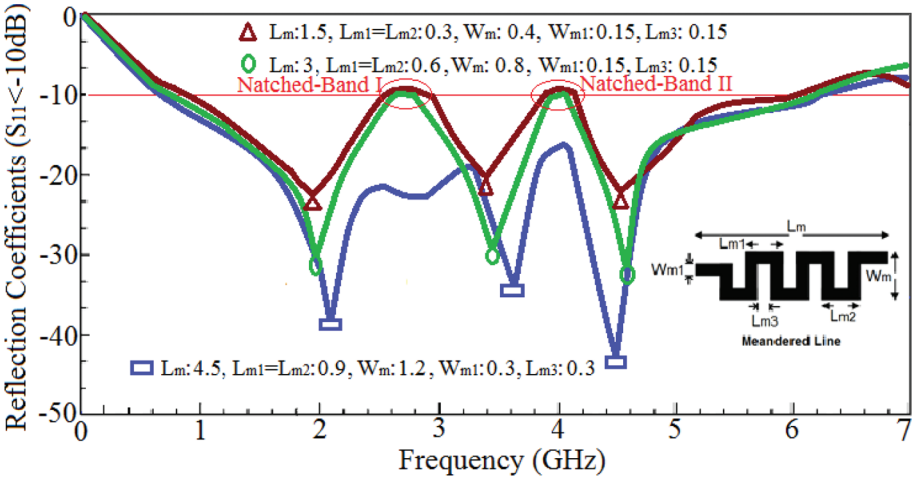

Figure 14. Antenna impedance bandwidth as a function of meandered strip-line size. All other structural parameters in **Table 1** remain fixed.

L_m	L_{m1} & L_{m2}	W_m	W_{m1}	L_{m3}	Notched-band
1.5	0.3	0.4	0.15	0.15	I: 2.55–2.95 GHz II: 3.85–4.15 GHz Impedance matching ≥ −20 dB
3	0.6	0.8	0.15	0.15	I: 2.6–2.8 GHz II: 3.95–4.05 GHz Impedance matching ≥ −30 dB
4.5	0.9	1.2	0.3	0.3	Eliminated Impedance matching ≥ −40 dB

Dimensions are in millimeters.

Table 4. Results of optimizing the meandered strip-line feed.

To summarize, a simple and effective technique has been demonstrated to extend the impedance bandwidth of patch antennas. This involves embedding three slits and exciting the antenna through a meandered strip-line. The radiating surface of the antenna is loaded with two inverted U-shape slits that are placed on either side of an H-shape slit. The antenna essentially behaves as a CRLH-TL structure. The antenna is shown to provide a fractional bandwidth of 223.27%, a maximum gain of 5.35 dBi and radiation efficiency of 84.12% at 4.45 GHz. Its radiation characteristics are similar to a monopole antenna. The proposed antenna should provide reliable wireless communication across UHF, L, S and C-bands.

Acknowledgements

The authors would like to give their special thanks to faculty of microelectronics for the financial supports.

Author details

Mohammad Alibakhshikenari[1]*, Mohammad Naser-Moghadasi[2], Ramazan Ali Sadeghzadeh[3], Bal Singh Virdee[4] and Ernesto Limiti[1]

*Address all correspondence to: Alibakhshikenari@ing.uniroma2.it

1 Department of Electronic Engineering, University of Rome Tor Vergata, Rome, Italy

2 Faculty of Engineering, Science and Research Branch, Islamic Azad University, Tehran, Iran

3 Faculty of Electrical Engineering, K. N. Toosi University of Technology, Tehran, Iran

4 London Metropolitan University, Center for Communications Technology, London, UK

References

[1] C.Y.D. Sim, F.R. Cai, and Y.P. Hsieh, "Multiband slot-ring antenna with single-and dual-capacitive coupled patch for wireless local area network/worldwide interoperability for microwave access operation", *IET Microw. Antenn. Propag. Lett.*, 2011; 5(15): 1830–1835. DOI: 10.1049/iet-map.2010.0462

[2] M. Alibakhshi-Kenari, M. Naser-Moghadasi, R.A. Sadeghzadeh, B.S. Virdee, and E. Limiti, "Dual-band RFID tag antenna based on the Hilbert-curve fractal for HF and UHF applications", *IET Circuits Dev. Sys.*, 2016; 10(2): 140–146. DOI: 10.1049/iet-cds.2015.0221

[3] J. William and R. Nakkeeran, "A new UWB slot antenna with rejection of WiMax and WLAN bands", *Appl. Comp. Electro. Soc. (ACES) J.*, 2010; 25(9): 787–793.

[4] S. Noghanian and M.K. Jung, "Ultra wide band planar slot antenna", *J. Electromagn. Waves Appl.*, 2008; 22(8–9): 1299–1308. DOI: 10.1163/156939308784158869

[5] M. Alibakhshi-Kenari, M. Naser-Moghadasi, and R.A. Sadeghzadah, "Bandwidth and radiation specifications enhancement of monopole antennas loaded with split ring resonators", *IET Microw. Antenn. P*, 2015; 9(14): 1487–1496. DOI: 10.1049/iet-map.2015.0172

[6] M. Alibakhshi-Kenari, M. Naser-Moghadasi, and R.A. Sadeghzadah, "The resonating MTM based miniaturized antennas for wide-band RF-microwave systems", *Microw. Opt. Technol. Lett.*, 2015; 57(10): 2339–2344. DOI: 10.1002/mop.29328

[7] M. Alibakhshi-Kenari, "Introducing the new wideband small plate antennas with engraved voids to form new geometries based on CRLH MTM-TLs for wireless applications", *Int. J. Microw. Wirel. Technol.*, 2014; 6(6): 629–637.

[8] M. Alibakhshi-Kenari, "A new compact UWB traveling-wave antenna based on CRLH-TLs for embedded electronic systems", *Int. J. Microw. Wirel. Technol.*, 2014: 1–4. DOI: 10.1017/S1759078714001020

[9] M. Alibakhshi-Kenari, "Printed planar patch antennas based on metamaterial", *Int. J. Elect. Lett.*, 2014; 2(1): 37–42. DOI: 10.1080/21681724.2013.874042

[10] H.-W. Liu, C.-H. Ku, and C.-F. Yang, "Novel CPW-fed planar monopole antenna for WiMAX/WLAN applications", *IEEE Antenn. Wirel. Propag. Lett.*, 2010; 9: 240–243. DOI: 10.1109/LAWP.2010.2044860

[11] Mohammad Alibakhshi-Kenari, Mohammad Naser-Moghadasi, R. A. Sadeghzadeh, Bal S. Virdee and Ernesto Limiti, "Traveling-Wave Antenna Based on Metamaterial Transmission Line Structure for Use in Multiple Wireless Communication Applications", AEUE Elsevier- International Journal of Electronics and Communications, Volume 70, Issue 12, December 2016, Pages 1645–1650.

[12] X.-L. Ma, W. Shao, and G.-Q. He, "A novel dual narrow band-notched CPW-Fed UWB slot antenna with parasitic strips", *Appl. Comp. Electro. Soc. (ACES) J.*, 2012; 27(7): 581–586.

[13] A. Sharma and G. Singh, "Design of single pin shorted three-dielectric-layered substrates rectangular patch microstrip antenna for communication systems", *Prog. Electromagn. Res. Lett.*, 2008; 2: 157–165.

[14] P.B.A. Fechine, A. Távora, L.C. Kretly, A.F.L. Almeida, M.R.P. Santos, F.N.A. Freire, and A.S. B. Sombra, "Microstrip antenna on a high dielectric constant substrate: $BaTiO_3$ (BTO)-$CaCu_3Ti_4O_{12}$ (CCTO) composite screen-printed thick films", *J. Elect. Mater.*, 2006; 35(10): 1848–1856.

[15] A. Pirhadi, H. Bahrami, and A. Mallahzadeh, "Electromagnetic band gap (EBG) superstrate resonator antenna design for monopulse radiation pattern", *Appl. Comp. Electro. Society (ACES) J.*, 2012; 27(11): 908–917.

[16] K.L. Chung and S. Chaimool, "Broadside gain and bandwidth enhancement of microstrip patch antenna using a MNZ-metasurface", *Microw. Opt. Technol. Lett.*, 2012; 54(2): 529–532.

[17] M. Alibakhshi-Kenari, M. Naser-Moghadasi, R.A. Sadeghzadeh, "Composite right-left handed based-antenna with wide applications in very-high frequency–ultra-high frequency bands for radio transceivers", *IET Microw. Antenn. P*, 2015; 9(15): 1713–1726. DOI: 10.1049/iet-map.2015.0308

[18] M. Alibakhshi-Kenari and M. Naser-Moghadasi, "Novel UWB miniaturized integrated antenna based on CRLH metamaterial transmission lines", *AEUE—Int. J. Elect. Commun.*, 2015; 69(8): 1143–1149.

[19] M. Alibakhshi-Kenari, M. Naser-Moghadasi, B.S. Virdee, A. Andújar, and J. Anguera, "Compact antenna based on a composite right/left handed transmission line", *Microw. Opt. Technol. Lett.*, 2015; 57(8): 1785–1788. DOI: 10.1002/mop.29191

[20] H.-W. Lai, K.-M. Luk, "Wideband patch antenna fed by printed meandering strip", *Microw. Opt. Technol. Lett.*, 2008; 50(1): 188–192.

[21] ANSYS®, High Frequency Structural Simulator (HFSS). ANSYS, Inc., USA.

[22] G.V. Eleftheriades, A. Grbic, and M. Antoniades, "Negative-refractive-index transmission-line metamaterials and enabling electromagnetic applications", *Proc. IEEE Antenn. Propag. Int. Symp.*, 2004: 1399–1402.

[23] A. Lai, C. Caloz, and T. Itoh, "Composite right/left-handed transmission line metamaterials", *IEEE Microw. Mag.*, 2004; 5(4): 34–50.

[24] C.-J. Lee, K.M.K.H. Leong, and T. Itoh, "Composite right/left-hand-handed transmission line based compact resonant antennas for RF module integration", *IEEE Trans. Antenn. Propag.*, 2006; 54(8): 2283–2291.

[25] C. Caloz and T. Itoh, "Application of the transmission line theory of left-handed (LH) materials to the realization of a microstrip 'LH line'", *Proc. IEEE Antenn. Propag. Soc. Int. Symp.*, 2002; 2: 412–415.

[26] Christophe Caloz and Tatsuo Itoh, "Electromagnetic Metamaterials: Transmission Line Theory and Microwave Applications", ISBN: 978-0-471-66985-2, 376 pages, December 2005, Wiley-IEEE Press.

[27] A. Sanada, C. Caloz, and T. Itoh, "Planar distributed structure with negative refractive index", *IEEE Trans. Microw. Theory Tech.*, 2004; 52(4): 1252–1263.

[28] C. Caloz, T. Itoh, and A. Rennings, "CRLH traveling-wave and resonant metamaterial antennas", *Antenn. Propag. Magazine*, 2008; 50(5): 25–39.

[29] Bonache, J., Gil, I., Garcıa-Garcıa, J., and Martın, F., "New microstrip filters based on complementary split rings resonators", *IEEE Trans. Microw. Theory Tech.*, 2006; 54: 265–271.

[30] Niu, J.-X., "Dual-band dual-mode patch antenna based on resonant-type metamaterial transmission line", *Electron. Lett.*, 2010; 46: 266–268.

[31] Y. Sun, G. Wen, P. Wang, Y. Huang, and Z. Du, "A compact printed end-fire antenna for radio frequency identification (RFID) handheld reader", *Appl. Comp. Electro. Soc. (ACES) J.*, 2013; 28(1): 71–76.

[32] C.-Y. Pan, T.-S. Horng, W.-S. Chen, and C.-H. Huang, "Dual wideband printed monopole antenna for WLAN/WiMAX applications", *IEEE Antenn. Wirel. Propag. Lett.*, 2007; 6: 149–151.